Advances in Nano Research, *Vol. 19, No. 5 (2025) 439-451*
https://doi.org/10.12989/anr.2025.19.5.439

Multi-physical field effects on wave dispersion characteristics of fluid-conveying triple-walled boron nitride nanotubes

Farzad Ebrahimi*[1], Marzieh Dehghan[2] and Ali Seyfi[3]

[1]*Department of Mechanical Engineering, Faculty of Engineering, Imam Khomeini International University, Qazvin, Iran*
[2]*Department of Mechanical Engineering, University of Technology Sydney, Sydney, Australia*
[3]*Department of Mechanical Engineering, Amirkabir University of Technology, Tehran, Iran*

(*Received February 18, 2025, Revised November 1, 2025, Accepted November 3, 2025*)

Abstract. The characterization of wave dispersion behavior can be helpful to predict the mechanical behavior of nanoscale structures, which can be used in nanoelectromechanical systems (NEMs). NEMs is a rapidly growing field that has seen multiple applications (e.g. sensors, actuators) in various areas such as electronics and healthcare. In this paper, wave dispersion response of fluid-conveying triple-walled boron nitride nanotubes (TWBNNTs) lying on viscoelastic medium under multi-physical fields is examined based on nonlocal strain gradient theory (NSGT). The TWBNNTs is modeled on the basis of the classic cylinder shell theory. The small-size impacts are considered by employing the NSGT. The governing equations are developed applying Hamilton's principle. The obtained results of present research are validated with available investigation in the literature. A comparison with the benchmark curves shows near one-to-one agreement of the nonlocal predictions in the low-k regime, with the local model underestimating the nondimensional frequency as wave number increases. The influences of different parameters like geometry, Knudsen number, viscoelastic medium, fluid velocity, multi-physical fields on the propagated waves in the studying structures are evaluated comprehensively.
Keywords: classical shell theory; fluid-conveying structure; nonlocal strain gradient theory; triple-walled boron nitride nanotubes; wave dispersion characteristics

1. Introduction

Since discovery of boron nitride nanotubes (BNNTs) in 1995, it attracted attention of many researchers in last decade. BNNTs have same atomic structure with carbon nanotubes (CNTs) whereas BNNTs have better resistance to oxidation at high temperatures (>900℃) and more stability. BNNTs are in crystalline and amorphous forms and have strong piezoelectric property. BNNTs unlike CNTs are chirality-independent which are considered as semi-conducting materials. These properties make them a fresh selection for producing actuators and sensors and high temperature equipment and smart control applications. Also, a controversial application is focused Ultrasound BNNT in which can improve drug transfer and concentrating drug at a specific location (Thibeault *et al*. 2015). The main properties of BNNTs and CNTs is indicated in Fig. 1. With the growth of the knowledge and reporting the different investigation on mechanical analysis of nanoscale structure, it can be found that the results of investigations which used classical theory is not accurate. Due to inaccuracy of classic mechanical theories in predicting mechanical response of nanoscale structures, scientists have developed non-classical mechanical theories including nonlocal elasticity theory (NET), modified couple stress theory (MCST), nonlocal strain gradient theory (NSGT), modified strain gradient theory (MSGT) and etc. The results of new investigations indicated that the small-scale effect is not take into account based on classical theories and it makes such theories inaccurate. However, the obtained results of the proposed theories are more accurate than classical theories (Ebrahimi *et al*. 2019a, b, c, 2023). For example, Ebrahimi and Seyfi (2022) studied the influence of nonlocal parameter on wave dispersion response of an embedded functionally graded piezoelectric nanobeam under electric field. Here, the small-scale effect is also considered based on NET. Seyfi *et al*. (2024) employed NET to assess the torsional vibrational behavior of non-circular auxetic nanorod. Recently, stability analysis of imperfect graphene platelets-strengthened composite microshells was performed by Taghizadeh *et al*. (2025) in the framework of MCST. Nonlinear static and dynamic characteristics of fluid-conveying CNTs-reinforced microshells exposed to 2D magnetic field were surveyed by Sobhy (2025) based on MCST. Moreover, NSGT was used by Esen *et al*. (2025) to analyze the buckling and vibration response of porous sandwich higher-order nanoscale plate.

In last two decades, several investigations have been performed on behavior of CNTs and BNNTs (Ebrahimi and Seyfi, 2023, Seyfi *et al*. 2022). BNNTs can be classified in single, double and multi walled nanotubes. In recent years, researchers studied buckling, vibration and wave propagation of single-walled boron nitride nanotubes (SWBNNTs) or double-walled boron nitride nanotubes (DWBNNTs) or multi-walled boron nitride nanotubes (MWBNNTs). As an

*Corresponding author, Ph.D., Professor,
E-mail: febrahimy@eng.ikiu.ac.ir

ISSN: 2287-237X (Print), 2287-2388 (Online)

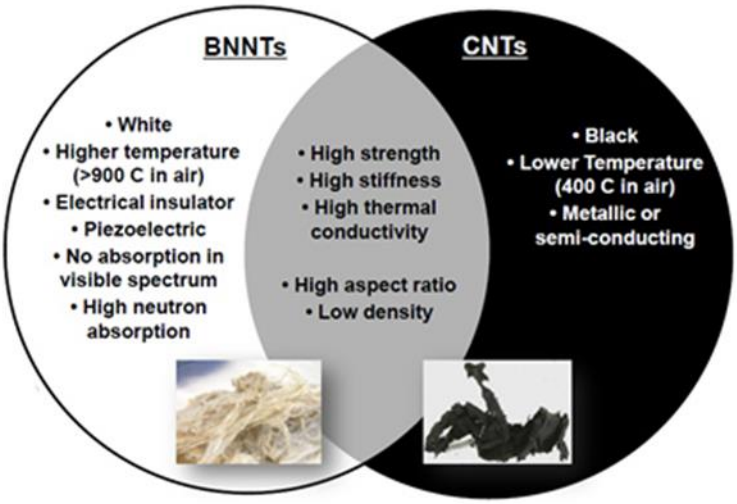

Fig. 1 Comparison between BNNTs and CNTs properties (Jakubinek *et al*. 2015)

instance of SWBNNTs, nonlinear vibration and stability of BNNT-reinforced composite microtube embedded in an elastic foundation exposed to electro-thermal loadings is probed by Arani *et al*. (2012). In another attempt, Arani and Roudbari (2014) investigated the impact of Knudsen-dependent fluid flow on wave dispersion phenomenon of SWBNNTs lying on viscoelastic substrate based on Euler-Bernoulli beam theory and nonlocal piezoelasticity theory. Thermal dynamic analysis of armchair BNNT was carried out by Chandra *et al*. (2015) with help of molecular dynamics simulations. The numerical simulation is conducted by Yan *et al*. (2017) to simulate vibrational behavior of SWBNNTs using Tersoff-Brenner potential. The super-harmonic and sub-harmonic resonance of BNNTs-strengthened composite beams subjected to internal thermal source was evaluated by Taati and Ahmadian (2023). Abdellahi *et al*. (2024) utilized differential quadrature method (DQM) to solve dynamic problem of BNNTs-strengthened piezo-electric actuators based on Timoshenko beam theory. As an instance of DWBNNTs, electronic and vibrational properties of zigzag DWBNNTs were investigated by Aydin (2013). Based on Timoshenko beam theory, Ghorbanpour-Arani *et al*. (2017) studied the propagation of waves in fluid-conveying double DWBNNTs rested on viscoelastic medium. Instability response of fluid-conveying hybrid-nanotube in the thermal environment and under magnetic field was explored by Sedighi *et al*. (2020) based on stress-driven nonlocal theory. The effect of thermal environment was examined by Roodgar Saffari *et al*. (2022) on frequency analysis of fluid-conveying DWBNNTs in the framework of first-order shear deformation theory.

As an instance of MWBNNTs, Mohammadimehr *et al*. (2015) implemented DQM to solve natural frequency problem of fluid-conveying triple-walled BNNTs (TWBNNTs) resting on viscoelastic foundation. Ansari *et al*. (2017) examined different boundary conditions effects on the vibrational behavior of concentric MWBNNTs and multi-walled CNTs using finite element method. The buckling analysis of concentric MWBNNTs subjected to the compressive loadings is discussed by Nikkar *et al*. (2019) exerting FEM. Choyal and Kundalwal (2020) predicted temperature-dependent transversely isotropic elastic characteristics of MWBNNTs by utilizing molecular dynamics simulations. the optical, electrical, and structural properties of SWBNNTs, DWBNNTs and MWBNNTs were examined by Badehian and Vatankhah (2022) by employing density functional theory. Wave dispersion in fluid-conveying nanotubes governs how axial disturbances, structural instabilities, and coupled electro-magneto-thermal fields travel and attenuate along the conduit. Reliable dispersion predictions are therefore essential for designing nanoelectro-mechanical (NEMS) elements where the “tube-as-channel” simultaneously acts as a structural member and a signal/transport pathway—e.g., flow-sensing, actuation, and high-frequency filtering. BNNTs are especially attractive because they combine high thermal stability, oxidation resistance, and intrinsic piezoelectricity while remaining semiconducting and chirality-independent, which supports robust transduction at elevated temperatures. These attributes make them strong candidates for sensors/actuators in harsh environments and smart-control hardware in healthcare and electronics. In practice, dispersion characteristics dictate comfort margins against flow-induced vibration and flutter in nanochannels, the bandwidth of piezoelectric signal transmission along tubular interconnects, and the stability of integrated nanofluidic lines embedded in viscoelastic hosts (e.g., polymer substrates or biological media). Tunability with external electric, magnetic, and thermal fields further enables on-demand reconfiguration of propagation speed and attenuation—useful for adaptive filters, threshold sensors, and precision drug-delivery micro-lines that rely on guided-wave control.

To our knowledge, no prior study has analyzed wave dispersion in fluid-conveying TWBNNTs resting on a viscoelastic foundation under simultaneous electro-magneto-thermal loading within a NSGT coupled to classical shell kinematics. Our formulation captures (i) concurrent nonlocality and strain-gradient size effects via the parameters e_0a and l, (ii) inter-wall van der Waals coupling for the triple-wall system, (iii) rarefaction/Knudsen corrections to

Table 1 The material properties of BNNTs (Salehi-Khojin and Jalili, 2008)

Property	Unit	Value
Mass Density	Kg m^{-3}	$\rho = 3487$
Elastic properties	GPa	$c_{11} = 2035, c_{22} = 2035,$ $c_{33} = 2035, c_{12} = 692,$ $c_{13} = 692, c_{23} = 692,$ $c_{44} = 672, c_{66} = 672$
Piezoelectric properties	C/m^2	$e_{31} = 0, \quad e_{33} = 0.95,$ $e_{15} = 0$
Dielectric properties	-	$\frac{\epsilon_{11}}{\epsilon_0} = 1250,$ $\frac{\epsilon_{22}}{\epsilon_0} = 1250,$ $\epsilon_{33}/\epsilon_0 = 1250$
Thermal properties	10^5 NKm^{-2}	$\beta_1 = 4.74, \beta_3 = 4.53$

the internal flow through a velocity-correction factor, and (iv) Winkler–Pasternak–damping substrate effects. We validate the wave-frequency predictions against a benchmark nonlocal shell model verified by molecular dynamics (Fig. 3), and then deliver a comprehensive parametric study quantifying how fluid velocity/density, Knudsen number, foundation parameters, and external fields modulate phase velocity. This specific combination of structure (TWBNNT), physics (electro-magneto-thermal plus rarefied internal flow), and foundation modeling within NSGT has not been reported previously.

2.Theory and formulation

The NSGT can be developed to BNNTs accounting for the elastic, magnetic and electric filed. So that elastic, electric field for a reference point depend not only on elastic and electric characteristics at the same point but also on all other points of the body. Basic relationships for BNNTs subjected to thermal, magnetic and electric fields are written in terms of nonlocal parameter ($e_0 a$) and length scale parameter (l) (Salehi-Khojin and Jalili, 2008):

$$(1-(e_0a)^2\nabla^2)\begin{Bmatrix}\sigma_{xi}\\ \sigma_{\theta i}\\ \sigma_{x\theta i}\end{Bmatrix} = (1-l^2\nabla^2)\left\{\begin{bmatrix}\tilde{c}_{11} & \tilde{c}_{12} & 0\\ \tilde{c}_{21} & \tilde{c}_{22} & 0\\ 0 & 0 & \tilde{c}_{66}\end{bmatrix}\begin{Bmatrix}\varepsilon_{xi}\\ \varepsilon_{\theta i}\\ \gamma_{x\theta i}\end{Bmatrix} - \begin{bmatrix}0 & 0 & \tilde{e}_{31}\\ 0 & 0 & \tilde{e}_{32}\\ 0 & 0 & \tilde{e}_{33}\end{bmatrix}\begin{Bmatrix}E_{xi}\\ E_{\theta i}\\ E_{zi}\end{Bmatrix}\right\} - \begin{bmatrix}\tilde{\beta}_1\\ \tilde{\beta}_2\\ 0\end{bmatrix}\Delta T \quad (1)$$

$$(1-(e_0a)^2\nabla^2)\begin{Bmatrix}D_{xi}\\ D_{\theta i}\\ D_{Zi}\end{Bmatrix} = (1-l^2\nabla^2)\left\{\begin{bmatrix}0 & 0 & 0\\ 0 & 0 & 0\\ \tilde{e}_{31} & \tilde{e}_{32} & \tilde{e}_{33}\end{bmatrix}\begin{Bmatrix}\varepsilon_{xi}\\ \varepsilon_{\theta i}\\ \gamma_{x\theta i}\end{Bmatrix} - \begin{bmatrix}\tilde{\in}_{11} & 0 & 0\\ 0 & \tilde{\in}_{22} & 0\\ 0 & 0 & \tilde{\in}_{33}\end{bmatrix}\begin{Bmatrix}E_{xi}\\ E_{\theta i}\\ E_{zi}\end{Bmatrix}\right\} + \begin{bmatrix}0\\ 0\\ \tilde{p}_3\end{bmatrix}\Delta T \quad (2)$$

where $\nabla^2 = \frac{\partial^2}{\partial z^2} + \frac{1}{R^2}\frac{\partial^2}{\partial \theta^2} + \frac{1}{R}\frac{\partial}{\partial R} + \frac{\partial}{\partial R^2}$. As well as, $\tilde{c}_{ij}, \tilde{e}_{ij}$, $\tilde{\beta}_1$, $\tilde{p}_3$ and $\tilde{\in}_{ij}$ denote the reduced coefficients BNNT that are formulated as:

$$\tilde{\in}_{11}=\in_{11},\ \tilde{\in}_{33}=\in_{33}-\frac{{e_{33}}^2}{c_{33}},$$
$$\tilde{e}_{31} = e_{31} - \frac{c_{13}e_{33}}{c_{33}},\ \tilde{p}_3 = p_3 + \frac{\beta_3 e_{33}}{c_{33}},\ \tilde{\beta}_1 = \beta_1 - \frac{c_{13}\beta_3}{c_{33}} \quad (3)$$
$$\tilde{c}_{66} = c_{66},\ \tilde{c}_{11} = c_{11} - \frac{{c_{13}}^2}{c_{33}},\ \tilde{c}_{12} = c_{12} - \frac{{c_{13}}^2}{c_{33}}$$

where in these equations:

$$\{A_{11} \quad A_{12} \quad A_{66}\} = \{h\tilde{c}_{11} \quad h\tilde{c}_{12} \quad h\tilde{c}_{66}\} \quad (4)$$

$$\{D_{11} \quad D_{12} \quad D_{66}\} = \left\{\frac{h^3\tilde{c}_{11}}{12} \quad \frac{h^3\tilde{c}_{12}}{12} \quad \frac{h^3\tilde{c}_{66}}{12}\right\} \quad (5)$$

$$E_{31} = \int_{-\frac{h}{2}}^{\frac{h}{2}} \tilde{e}_{31}\beta\, sin(\beta z)dz \quad (6)$$

$$X_{11} = \int_{-\frac{h}{2}}^{\frac{h}{2}} \tilde{\in}_{11}\, cos^2(\beta z)dz \quad (7)$$

$$X_{22} = \int_{-\frac{h}{2}}^{\frac{h}{2}} \tilde{\in}_{11}\left[\frac{cos(\beta z)}{R+z}\right]^2 dz \quad (8)$$

$$X_{33} = \int_{-\frac{h}{2}}^{\frac{h}{2}} \tilde{\in}_{33}\,[\beta\, sin(\beta z)]^2 dz \quad (9)$$

$$T_{11} = \int_{-\frac{h}{2}}^{\frac{h}{2}} \tilde{\mu}_{11}\, cos^2(\beta z)dz \quad (10)$$

$$T_{22} = \int_{-\frac{h}{2}}^{\frac{h}{2}} \tilde{\mu}_{22}\left[\frac{cos(\beta z)}{R+z}\right]^2 dz \quad (11)$$

$$T_{33} = \int_{-\frac{h}{2}}^{\frac{h}{2}} \tilde{\mu}_{33}\,[\beta\, sin(\beta z)]^2 dz \quad (12)$$

The constant material properties of BNNTs are given in Table 1. Moreover, the electric field is formulated in the following form:

$$E_{xi} = -\frac{\partial\widetilde{\Phi}}{\partial x} = cos(\beta z)\frac{\partial\Phi_i}{\partial x} \quad (13)$$

$$E_{\theta i} = -\frac{1}{R_i+z}\frac{\partial\widetilde{\Phi}}{\partial\theta} = \frac{cos(\beta z)}{R+z}\frac{\partial\Phi_i}{\partial\theta} \quad (14)$$

$$E_{zi} = -\frac{\partial\widetilde{\Phi}}{\partial z} = -\beta\, sin(\beta z)\Phi_i - \frac{2\phi_0}{h} \quad (15)$$

where $\widetilde{\Phi}$ is electric potential which can be presented in terms of variation of electric potential (Φ) and its initial value ($\varphi 0$) (Salehi-Khojin and Jalili 2008):

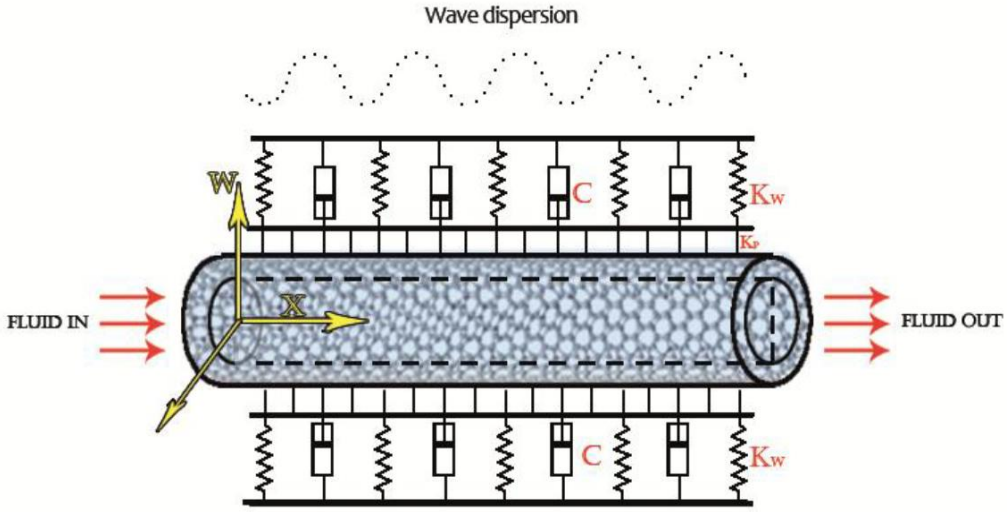

Fig. 2 Schematic of fluid-conveying BNNT lying on a viscoelastic substrate (Salehi-Khojin and Jalili, 2008)

$$\widetilde{\Phi}(x,\theta,z,t) = -cos(\beta z)\Phi(x,\theta,t) + \frac{2z\varphi_0}{h}, \quad \beta = \frac{\pi}{h} \tag{16}$$

To better physical understanding from the studying subject, the Fig. 2 is provided. Fig. 2 illustrates the schematic of a fluid-conveying BNNT rested on viscoelastic medium.

The displacement fields of BNNTs are modeled according to Love's shell theory (Gopalakrishnan and Narendar, 2013):

$$u_1(x,\theta,z,t) = U(x,\theta,t) - z\frac{\partial W(x,\theta,t)}{\partial x}, \tag{17}$$

$$u_2(x,\theta,z,t) = V(x,\theta,t) - z\frac{1}{R}\frac{\partial W(x,\theta,t)}{\partial y}, \tag{18}$$

$$u_3(x,\theta,z,t) = W(x,\theta,t) \tag{19}$$

Also, the non-zero strain relations are written as (Gopalakrishnan and Narendar, 2013):

$$\varepsilon_{xi} = \frac{\partial U_i}{\partial x} - z\frac{\partial^2 W_i}{\partial x^2}, \tag{20}$$

$$\varepsilon_{\theta i} = \frac{z}{R_i^2}\left(\frac{\partial V_i}{\partial \theta} - \frac{\partial^2 W}{\partial \theta^2}\right) + \frac{1}{R_i}\left(W_i + \frac{\partial V_i}{\partial \theta}\right), \tag{21}$$

$$\gamma_{x\theta i} = \frac{1}{R_i}\left(W_i + \frac{\partial U_i}{\partial \theta}\right) + \frac{\partial V_i}{\partial x} - \frac{z}{R_i}\left(2\frac{\partial^2 W}{\partial x \partial \theta} - \frac{\partial V_i}{\partial x}\right), \tag{22}$$

Subscript i shows layer number (1, 2 and 3). Normal loads and bending moments are presented as follow:

$$(N_{xi} \quad N_{\theta i} \quad N_{x\theta i}) = \int_{-\frac{h}{2}}^{\frac{h}{2}} (\sigma_{xi} \quad \sigma_{\theta i} \quad \sigma_{x\theta i})\, dz \tag{23}$$

$$(M_{xi} \quad M_{\theta i} \quad M_{x\theta i}) = \int_{-\frac{h}{2}}^{\frac{h}{2}} (\sigma_{xi} \quad \sigma_{\theta i} \quad \sigma_{x\theta i}) z\, dz \tag{24}$$

By substituting Eqs. (13) to (24) into Eqs. (1-2), the following equations can be obtained:

$$\begin{aligned} &N_{xi} - \mu^2\nabla^2 N_{xi} = A_{11}\frac{\partial U_i}{\partial x} + \frac{A_{12}}{R_i}\left(\frac{\partial V_i}{\partial \theta} + W_i\right) \\ &-l^2 A_{11}\left(\frac{1}{{R_i}^2}\frac{\partial^3 U_i}{\partial \theta^2 \partial x} + \frac{\partial^3 U_i}{\partial x^3}\right) \\ &-l^2 A_{12}\left(\frac{1}{{R_i}^3}\frac{\partial^3 V_i}{\partial \theta^3} + \frac{1}{R_i}\frac{\partial^3 V_i}{\partial \theta \partial x^2} + \frac{1}{{R_i}^3}\frac{\partial^2 W_i}{\partial \theta^2} + \frac{1}{R_i}\frac{\partial^2 W_i}{\partial x^2}\right) \\ &+N_{Mxi} + N_{Exi} + N_{Txi} \end{aligned} \tag{25}$$

$$\begin{aligned} &N_{\theta i} - \mu^2\nabla^2 N_{\theta i} = A_{12}\frac{\partial U_i}{\partial x} + \frac{A_{11}}{R_i}\left(\frac{\partial V_i}{\partial \theta} + W_i\right) \\ &-l^2 A_{12}\left(\frac{1}{{R_i}^2}\frac{\partial^3 U_i}{\partial \theta^2 \partial x} + \frac{\partial^3 U_i}{\partial x^3}\right) - A_{11}l^2\left(\frac{1}{{R_i}^3}\frac{\partial^3 V_i}{\partial \theta^3}\right. \\ &\left.+\frac{1}{R_i}\frac{\partial^3 V_i}{\partial \theta \partial x^2} + \frac{1}{{R_i}^3}\frac{\partial^2 W_i}{\partial \theta^2} + \frac{1}{R_i}\frac{\partial^2 W_i}{\partial x^2}\right) \\ &+N_{M\theta i} + N_{E\theta i} + N_{T\theta i} \end{aligned} \tag{26}$$

$$\begin{aligned} &N_{x\theta i} - e_0 a^2\nabla^2 N_{x\theta i} = A_{66}\left(\frac{\partial V_i}{\partial x} + \frac{1}{R_i}\frac{\partial U_i}{\partial \theta}\right) \\ &-l^2 A_{66}\left(\frac{1}{{R_i}^2}\frac{\partial^3 V_i}{\partial x \partial \theta^2} + \frac{\partial^3 V_i}{\partial x^3} + \frac{1}{{R_i}^3}\frac{\partial^3 U_i}{\partial \theta^3} + \right. \\ &\left.\frac{1}{R_i}\frac{\partial^3 U_i}{\partial \theta \partial x^2}\right) \end{aligned} \tag{27}$$

$$\begin{aligned} &M_{xi} - e_0 a^2\nabla^2 M_{xi} \\ &= -D_{11}\frac{\partial^2 W_i}{\partial x^2} - \frac{D_{12}}{{R_i}^2}\left(\frac{\partial^2 W_i}{\partial \theta^2} - \frac{\partial V_i}{\partial \theta}\right) + E_{31}\Phi_i \\ &+l^2 D_{11}\left(\frac{1}{{R_i}^2}\frac{\partial^4 W_i}{\partial \theta^2 \partial x^2} + \frac{\partial^4 W_i}{\partial x^4}\right) \\ &+l^2 D_{12}\left(\frac{1}{{R_i}^2}\frac{\partial^4 W_i}{\partial x^2 \partial \theta^2} + \frac{1}{{R_i}^4}\frac{\partial^4 W_i}{\partial \theta^4}\right. \\ &\left.-\frac{1}{{R_i}^2}\frac{\partial^3 V_i}{\partial \theta \partial x^2} - \frac{1}{{R_i}^4}\frac{\partial^3 V_i}{\partial \theta^3}\right) \\ &-l^2 E_{31}\left(\frac{1}{{R_i}^2}\frac{\partial^2 \Phi_i}{\partial \theta^2} + \frac{\partial^2 \Phi_i}{\partial x^2}\right) \end{aligned} \tag{28}$$

$$M_{\theta i}-e_0a^2\nabla^2M_{\theta i}=-D_{12}\frac{\partial^2W_i}{\partial x^2}-\frac{D_{11}}{{R_i}^2}\left(\frac{\partial^2W_i}{\partial\theta^2}-\frac{\partial V_i}{\partial\theta}\right)+E_{31}\Phi_i+l^2D_{12}\left(\frac{1}{{R_i}^2}\frac{\partial^4W_i}{\partial\theta^2\partial x^2}+\frac{\partial^4W_i}{\partial x^4}\right)+l^2D_{11}(\frac{1}{{R_i}^2}\frac{\partial^4W_i}{\partial x^2\partial\theta^2}+\frac{1}{{R_i}^4}\frac{\partial^4W_i}{\partial\theta^4}-\frac{1}{{R_i}^2}\frac{\partial^3V_i}{\partial\theta\partial x^2}-\frac{1}{{R_i}^4}\frac{\partial^3V_i}{\partial\theta^3})-l^2E_{31}(\frac{1}{{R_i}^2}\frac{\partial^2\Phi_i}{\partial\theta^2}+\frac{\partial^2\Phi_i}{\partial x^2}\quad(29)$$

$$M_{x\theta i}-e_0a^2\nabla^2M_{x\theta i}=-\frac{D_{66}}{R_i}\left(\frac{2}{R_i}\frac{\partial^2W_i}{\partial\theta\partial x}-\frac{\partial V_i}{\partial x}\right)+l^2D_{66}(\frac{2}{{R_i}^2}\frac{\partial^4W_i}{\partial\theta\partial x^3}+\frac{2}{{R_i}^4}\frac{\partial^4W_i}{\partial\theta^3\partial x}-\frac{1}{{R_i}^2}\frac{\partial^3V_i}{\partial x^3}-\frac{1}{{R_i}^2}\frac{\partial^3W_i}{\partial x\partial\theta^2})\quad(30)$$

$$\int_{-\frac{h}{2}}^{\frac{h}{2}}cos(\beta z)[D_{xi}-e_0a^2\nabla^2D_{xi}]dz=X_{11}\frac{\partial\Phi_i}{\partial x}-l^2X_{11}(\frac{1}{{R_i}^2}\frac{\partial^3\Phi_i}{\partial x\partial\theta^2}+\frac{\partial^3\Phi_i}{\partial x^3})\quad(31)$$

$$\int_{-\frac{h}{2}}^{\frac{h}{2}}\frac{cos(\beta z)}{R_i+z}[D_{\theta i}-e_0a^2\nabla^2D_{\theta i}]dz=X_{22}\frac{\partial\Phi_i}{\partial\theta}-l^2X_{22}(\frac{1}{{R_i}^2}\frac{\partial^3\Phi_i}{\partial\theta^3}+\frac{\partial^3\Phi_i}{\partial\theta\partial x^2})\quad(32)$$

$$\int_{-\frac{h}{2}}^{\frac{h}{2}}\beta\,sin(\beta z)[D_{zi}-e_0a^2\nabla^2D_{zi}]dz=-E_{31}\frac{\partial^2W_i}{\partial x^2}-\frac{E_{31}}{{R_i}^2}\left(\frac{\partial^2W_i}{\partial\theta^2}-\frac{\partial V_i}{\partial\theta}\right)-X_{33}\Phi_i+l^2E_{31}(\frac{\partial^4W_i}{\partial x^4}+\frac{1}{{R_i}^2}\frac{\partial^4W_i}{\partial x^2\partial\theta^2})+E_{31}(\frac{1}{{R_i}^4}\frac{\partial^4W_i}{\partial\theta^4}+\frac{1}{{R_i}^2}\frac{\partial^2W_i}{\partial x^2\partial\theta^2}-\frac{1}{{R_i}^4}\frac{\partial^3V_i}{\partial\theta^3}-\frac{1}{{R_i}^2}\frac{\partial^3V_i}{\partial x^2\partial\theta})+l^2X_{33}(\frac{1}{{R_i}^2}\frac{\partial^2\Phi_i}{\partial\theta^2}+\frac{\partial^2\Phi_i}{\partial x^2})\quad(33)$$

3.Governing equations

To develop the nonlocal governing equations of BNNTs, Hamilton`s principle is employed in terms of strain energy (Π_{Si}), kinetic energy (Π_{Ki}) and work done by external force (Π_{Fi}):

$$\int_{t_1}^{t_2}\delta(\prod_{Ki}-(\prod_{Fi}+\prod_{Si})\,dt=0\quad(34)$$

Kinetic energy of BNNT is written as:

$$\prod_{Ki}=\tfrac{1}{2}\int_0^L\int_0^{2\pi}\left[I_1\left(\frac{\partial U_i}{\partial t}\right)^2+I_1\left(\frac{\partial V_i}{\partial t}\right)^2+I_1\left(\frac{\partial W_i}{\partial t}\right)^2\right]R_i d\theta dx\quad(35)$$

in which $I_1=\rho h$.

Elastic and electric strain energies are defined as:

$$\prod_{S1}=\frac{1}{2}\int_0^L\int_0^{2\pi}\begin{bmatrix}N_x\frac{\partial U_i}{\partial x}+\frac{N_\theta}{R_i}\left(\frac{\partial V_i}{\partial\theta}+W_i\right)\\+N_{x\theta}(\frac{\partial V_i}{\partial x}+\frac{1}{R_i}\frac{\partial U_i}{\partial\theta})\end{bmatrix}R_i d\theta dx-\frac{1}{2}\int_0^L\int_0^{2\pi}\begin{bmatrix}M_x\frac{\partial^2W_i}{\partial x^2}+\frac{M_\theta}{{R_i}^2}\left(\frac{\partial^2W_i}{\partial\theta^2}-\frac{\partial V_i}{\partial\theta}\right)\\+\frac{M_{x\theta}}{R_i}(\frac{2\partial^2W_i}{\partial x\partial\theta}-\frac{\partial V_i}{\partial x})\end{bmatrix}R_i d\theta dx\quad(36)$$

$$\prod_{S2}=-\frac{1}{2}\int_0^L\int_0^{2\pi}\int_{-\frac{h}{2}}^{\frac{h}{2}}\begin{bmatrix}and D_{xi}\,cos(\beta z)\frac{\partial\Phi_i}{\partial x}\\+D_{\theta i}\frac{cos(\beta z)}{R_i+z}\frac{\partial\Phi_i}{\partial\theta}\\and-D_{zi}(\beta\,sin(\beta z))\Phi_i\\+\frac{2\phi_0}{h}\end{bmatrix}R_i dz d\theta dx\quad(37)$$

Various forces including van der Waals force, thermo-magneto-electric field force are applied to BNNT. The work done by external forces is presented in terms of vertical induced forces by thermo-magneto-electric forces as (Salehi-Khojin and Jalili, 2008):

$$\prod_{F1}=\frac{1}{2}\int_0^L\int_0^{2\pi}\begin{bmatrix}(N_{Tx}+N_{Mx}\\+N_{Ex})\left(\frac{\partial W_i}{\partial t}\right)^2\end{bmatrix}R_i d\theta dx+\frac{1}{2}\int_0^L\int_0^{2\pi}\left[\frac{(N_{T\theta}+N_{M\theta}+N_{E\theta})}{R^2}\left(\frac{\partial W_i}{\partial\theta}\right)^2\right]R_i d\theta dx\quad(38)$$

The vertical induced forces are introduced as:

$$N_{Tx}=N_{T\theta}=\tilde{\beta}_1h\Delta T,\ N_{Ex}=N_{E\theta}=-2\tilde{e}_{31}\phi_0,\ N_{Mx}=N_{M\theta}=-2\tilde{q}_{31}\psi_0\quad(39)$$

The work done by force of magnetic fluid can be defined in terms of fluid density (ρ_f) and average velocity correction factor (VCF) (Abdollahian *et al*. 2013):

$$\prod_{F2}=\int_0^L\int_0^{2\pi}\left[-\frac{\rho_fR}{2}\left(\frac{\partial^2W}{\partial t^2}+2V_fVCF\frac{\partial^2W}{\partial t\partial x}+(V_fVCF)^2\frac{\partial^2W}{\partial x^2}\right)\right]Rd\theta dx\quad(40)$$

To evaluate the impact of fluid flow passing through a nanostructure, the Knudsen number (Kn) must be considered. VCF and rarefaction factor ($Cr(Kn)$) are formulated in terms of tangential momentum accommodation coefficient (σv) (Oveissi and Nahvi, 2015):

$$VCF=\frac{V_{\text{slip}}}{V_{no-\text{slip}}}=\frac{1}{Cr(Kn)}(4(\frac{2-\sigma_v}{\sigma_v})(\frac{Kn}{1-bKn})+1)\quad(41)$$

$$Cr(Kn)=\frac{1}{1+\alpha Kn}\quad(42)$$

$$\alpha=\frac{2}{\pi}\alpha_0[tan^{-1}(\alpha_1Kn^B)]\quad(43)$$

$$VCF=\frac{V_{\text{slip}}}{V_{no-\text{slip}}}=\frac{1}{Cr(Kn)}(4(\frac{2-\sigma_v}{\sigma_v})(\frac{Kn}{1-bKn})+1) \quad (44)$$

In addition, van der Waals force between interlayers is written as (Dong *et al*. 2008, Mitra and Gopalakrishnan, 2009):

$$p_{i(i+1)}=c(W_{i+1}-W_i) \quad (45)$$

$$p_{(i+1)(i)}=-\frac{R_i}{R_{i+1}}p_{(i)(i+1)} \quad (46)$$

where$p_{i(i+1)}$ and Wi denote force of the two neighboring layers and layer i's transverse displacement, respectively. Therefore, the force from layer 1 to layer 2 is computed as:

$$p_1=p_{12}=c(W_2-W_1) \quad (47)$$

Also, the reaction force is represented as follow:

$$p_{21}=-\frac{R_1}{R_2}p_{12} \quad (48)$$

$$\begin{aligned}p_2&=p_{23}+p_{21}=p_{23}-\frac{R_1}{R_2}p_{12}\\&=c(W_3-W_2)-c\frac{R_1}{R_2}(W_2-W_1)\end{aligned} \quad (49)$$

$$p_3=p_{34}+p_{32}=0-\frac{R_2}{R_3}p_{23}=-c\frac{R_2}{R_3}(W_3-W_2) \quad (50)$$

in which

$$c=\frac{320erg/cm^2}{0.16d^2},(d=0.145nm,1erg=10^{-7}j) \quad (51)$$

As a result, the work done by van der Waals force is expressed as:

$$\prod_{F3}{}^{(i)}=\int_0^{2\pi}\int_0^{L}p_i\,R_iW_i dxd\theta,(i=1,2,\dots,N) \quad (52)$$

The effect of various foundation types on mechanical behavior of structures have been investigated by different scientists. For more information, the interested readers can refer to Seyfi and Aghdam, 2023. In the current investigation, viscoelastic foundation is considered to be the structure foundation. This foundation consists of a linear layer (Winkler) and shear layer (Pasternak) and viscous damper. Work done by viscoelastic medium is formulated in terms of damping coefficient (*C*), Winkler coefficient (K_w), Pasternak coefficient (K_G) as (Zeighampour *et al*. 2018):

$$\prod_{F4}=\int_0^{2\pi}\int_0^{L}(K_wW_2-K_G\frac{\partial^2W_2}{\partial x^2}+C\frac{\partial W_2}{\partial t})R_3dxd\theta \quad (53)$$

By inserting the corresponding equations for each parameter in Hamilton's principle, coefficients variation of displacement fields is written as:

$$\delta U:\frac{\partial N_{xi}}{\partial x}+\frac{1}{R_i}\frac{\partial N_{x\theta i}}{\partial\theta}=I_1\frac{\partial^2U_i}{\partial t^2} \quad (54)$$

$$\delta V:\frac{\partial N_{x\theta i}}{\partial x}+\frac{1}{R_i}\frac{\partial N_{\theta i}}{\partial\theta}+\frac{1}{R_i}\frac{\partial M_{x\theta i}}{\partial x}+\frac{1}{{R_i}^2}\frac{\partial M_{\theta i}}{\partial\theta}=I_1\frac{\partial^2V_i}{\partial t^2} \quad (55)$$

$$\begin{aligned}&\delta W:\frac{\partial M_{xi}}{\partial x^2}+\frac{2}{R_i}\frac{\partial^2M_{x\theta i}}{\partial x\partial\theta}+\frac{1}{{R_i}^2}\frac{\partial^2M_{\theta i}}{\partial\theta^2}-\frac{N_{\theta i}}{R_i}-N_{x0}\frac{\partial^2W_i}{\partial x^2}\\&-\frac{N_{\theta0}}{{R_i}^2}\frac{\partial^2W_i}{\partial\theta^2}+\frac{\rho_fR_1}{2}\begin{pmatrix}\frac{\partial^2W_1}{\partial t^2}+2V_fVCF\frac{\partial^2W_1}{\partial t\partial x}\\+(2V_fVCF)^2\frac{\partial^2W_1}{\partial x^2}\end{pmatrix}\\&-P_i+K_wW_3-K_g\nabla^2W_3+C\frac{\partial W_3}{\partial t}=I_1\frac{\partial^2W_i}{\partial t^2}\end{aligned} \quad (56)$$

$$\delta\Phi:\int_{-h/2}^{h/2}\begin{bmatrix}\frac{\partial D_{xi}}{\partial x}cos(\beta z)+\frac{cos(\beta z)}{R_i+z}\frac{\partial D_{\theta i}}{\partial\theta}\\+D_{zi}\beta\,sin(\beta z)\end{bmatrix}dz=0 \quad (57)$$

in these equations $N_{x0}=N_{Ex}+N_{Mx}+N_{Tx}$ and $N_{\theta0}=N_{E\theta}+N_{M\theta}+N_{T\theta}$.

By coupling Eqs. (25) – (33) with Eqs. (54) – (57), the governing equation of multi-layer nanostructure can be derived as:

$$\begin{aligned}&A_{11}\frac{\partial^2U_i}{\partial x^2}+\frac{A_{12}}{R_i}\left(\frac{\partial^2V_i}{\partial x\partial\theta}+\frac{\partial W}{\partial x}\right)-A_{11}\frac{l^2}{{R_i}^2}\frac{\partial^4U_i}{\partial x^2\partial\theta^2}\\&-A_{11}l^2\frac{\partial^4U_i}{\partial x^4}-A_{12}\frac{l^2}{{R_i}^3}\frac{\partial^4V_i}{\partial x\partial\theta^3}-A_{12}\frac{l^2}{R_i}\frac{\partial^4V_i}{\partial x^3\partial\theta}\\&-A_{12}\frac{l^2}{{R_i}^3}\frac{\partial^3W_i}{\partial x\partial\theta^2}-A_{12}\frac{l^2}{R_i}\frac{\partial^3W_i}{\partial x^3}+\frac{A_{66}}{R_i}\frac{\partial^2V_i}{\partial x\partial\theta}+\frac{A_{66}}{{R_i}^2}\frac{\partial^2U_i}{\partial\theta^2}\\&-A_{66}\frac{l^2}{{R_i}^3}\frac{\partial^4V_i}{\partial x\partial\theta^3}-A_{66}\frac{l^2}{R_i}\frac{\partial^4V_i}{\partial x^3\partial\theta}-A_{66}\frac{l^2}{{R_i}^4}\frac{\partial^4U_i}{\partial\theta^4}\\&-A_{66}\frac{l^2}{{R_i}^2}\frac{\partial^4U_i}{\partial x^2\partial\theta^2}=\{1-e_0a^2\nabla^2\}(I_1\frac{\partial^2U_i}{\partial t^2})\end{aligned} \quad (58)$$

$$\begin{aligned}&A_{66}\frac{\partial^2V_i}{\partial x^2}+\frac{A_{66}}{R_i}\frac{\partial^2U_i}{\partial x\partial\theta}-A_{66}\frac{l^2}{{R_i}^2}\frac{\partial^4V_i}{\partial x^2\partial\theta^2}-A_{66}l^2\frac{\partial^4V_i}{\partial x^4}\\&-A_{66}\frac{l^2}{{R_i}^3}\frac{\partial^4U_i}{\partial x\partial\theta^3}-A_{66}\frac{l^2}{R_i}\frac{\partial^4U_i}{\partial x^3\partial\theta}+\frac{A_{12}}{R_i}\frac{\partial^2U_i}{\partial x\partial\theta}+\frac{A_{11}}{{R_i}^2}\frac{\partial^2V_i}{\partial\theta^2}\\&+\frac{A_{11}}{{R_i}^2}\frac{\partial W_i}{\partial\theta}-A_{12}\frac{l^2}{{R_i}^3}\frac{\partial^4U_i}{\partial x\partial\theta^3}-A_{12}\frac{l^2}{R_i}\frac{\partial^4U_i}{\partial x^3\partial\theta}-A_{11}\frac{l^2}{{R_i}^4}\frac{\partial^4V_i}{\partial\theta^4}\\&-A_{11}\frac{l^2}{{R_i}^2}\frac{\partial^4V_i}{\partial x^2\partial\theta^2}-A_{11}\frac{l^2}{{R_i}^4}\frac{\partial^3W_i}{\partial\theta^3}-A_{11}\frac{l^2}{{R_i}^2}\frac{\partial^3W_i}{\partial x^2\partial\theta}\\&-\frac{D_{66}}{{R_i}^2}\frac{2\partial^3W_i}{\partial x^2\partial\theta}+\frac{D_{66}}{{R_i}^2}\frac{\partial^2V_i}{\partial x^2}+2D_{66}\frac{l^2}{{R_i}^4}\frac{\partial^5W_i}{\partial x^2\partial\theta^3}\\&+2D_{66}\frac{l^2}{{R_i}^2}\frac{\partial^5W_i}{\partial x^4\partial\theta}-D_{66}\frac{l^2}{{R_i}^4}\frac{\partial^4V_i}{\partial x^2\partial\theta^2}-D_{66}\frac{l^2}{{R_i}^2}\frac{\partial^4V_i}{\partial x^4}\\&-\frac{D_{12}}{{R_i}^2}\frac{\partial^3W_i}{\partial x^2\partial\theta}-\frac{D_{11}}{{R_i}^4}\frac{\partial^3W_i}{\partial\theta^3}+\frac{D_{11}}{{R_i}^4}\frac{\partial^2V_i}{\partial\theta^2}+\frac{E_{31}}{{R_i}^2}\frac{\partial\Phi_i}{\partial\theta}\\&+D_{12}\frac{l^2}{{R_i}^4}\frac{\partial^5W_i}{\partial x^2\partial\theta^3}+D_{12}\frac{l^2}{{R_i}^2}\frac{\partial^5W_i}{\partial x^4\partial\theta}+D_{11}\frac{l^2}{{R_i}^6}\frac{\partial^5W_i}{\partial\theta^5}\\&+D_{11}\frac{l^2}{{R_i}^4}\frac{\partial^5W_i}{\partial x^2\partial\theta^3}-D_{11}\frac{l^2}{{R_i}^6}\frac{\partial^4V_i}{\partial\theta^4}-D_{11}\frac{l^2}{{R_i}^4}\frac{\partial^4V_i}{\partial x^2\partial\theta^2}\\&-E_{31}\frac{l^2}{{R_i}^4}\frac{\partial^3\Phi_i}{\partial\theta^3}-E_{31}\frac{l^2}{{R_i}^2}\frac{\partial^3\Phi_i}{\partial x^2\partial\theta}=\{1-e_0a^2\nabla^2\}(I_1\frac{\partial^2V_i}{\partial t^2})\end{aligned} \quad (59)$$

$$\begin{aligned}&-D_{11}\frac{\partial^4W_i}{\partial x^4}-\frac{D_{12}}{R^2}\frac{\partial^4W_i}{\partial x^2\partial\theta^2}+\frac{D_{12}}{R^2}\frac{\partial^3V_i}{\partial x^2\partial\theta}+E_{31}\frac{\partial^2\Phi_i}{\partial x^2}\\&+D_{11}\frac{l^2}{R^2}\frac{\partial^6W_i}{\partial x^4\partial\theta^2}+D_{11}l^2\frac{\partial^6W_i}{\partial x^6}+D_{12}\frac{l^2}{R^4}\frac{\partial^6W_i}{\partial x^2\partial\theta^4}\\&+D_{12}\frac{l^2}{R^2}\frac{\partial^6W_i}{\partial x^4\partial\theta^2}-D_{12}\frac{l^2}{R^4}\frac{\partial^5V_i}{\partial x^2\partial\theta^3}-D_{12}\frac{l^2}{R^2}\frac{\partial^5V_i}{\partial x^4\partial\theta}+\\&E_{31}\frac{l^2}{R^2}\frac{\partial^4\Phi_i}{\partial x^2\partial\theta^2}+E_{31}l^2\frac{\partial^4\Phi_i}{\partial x^4}-\frac{4D_{66}}{R^2}\frac{\partial^4W_i}{\partial x^2\partial\theta^2}+\frac{2D_{66}}{R^2}\frac{\partial^3V_i}{\partial x^2\partial\theta}\end{aligned} \quad (60)$$

$$
\begin{aligned}
&+4D_{66}\frac{l^2}{R^4}\frac{\partial^6 W_i}{\partial x^2\partial\theta^4}+4D_{66}\frac{l^2}{R^2}\frac{\partial^6 W_i}{\partial x^4\partial\theta^2}-2D_{66}\frac{l^2}{R^4}\frac{\partial^5 V_i}{\partial x^2\partial\theta^3}\\
&-2D_{66}\frac{l^2}{R^2}\frac{\partial^5 V_i}{\partial x^4\partial\theta}-\frac{D_{12}}{R^2}\frac{\partial^4 W_i}{\partial x^2\partial\theta^2}-\frac{D_{11}}{R^4}\frac{\partial^4 W_i}{\partial\theta^4}+\frac{D_{11}}{R^4}\frac{\partial^3 V_i}{\partial\theta^3}\\
&+\frac{E_{31}}{R^2}\frac{\partial^2\Phi_i}{\partial\theta^2}-\frac{A_{12}}{R}\frac{\partial U_i}{\partial x}-\frac{A_{11}}{R^2}\frac{\partial V_i}{\partial\theta}-\frac{A_{11}}{R^2}W_i+A_{12}\frac{l^2}{R^3}\frac{\partial^3 U_i}{\partial x\partial\theta^2}\\
&+A_{12}\frac{l^2}{R}\frac{\partial^3 U_i}{\partial x^3}+A_{11}\frac{l^2}{R^4}\frac{\partial^3 V_i}{\partial\theta^3}+A_{11}\frac{l^2}{R^2}\frac{\partial^3 V_i}{\partial x^2\partial\theta}+A_{11}\frac{l^2}{R^4}\frac{\partial^2 W_i}{\partial\theta^2}\\
&+A_{11}\frac{l^2}{R^2}\frac{\partial^2 W_i}{\partial x^2}-\{1-e_0a^2\nabla^2\}(\rho_f\frac{R}{2}(\frac{\partial^2 W_1}{\partial t^2}\\
&+2V_{nf}VCF\frac{\partial^2 W_1}{\partial t\partial x}+(V_{nf}VCF)^2\frac{\partial^2 W_1}{\partial x^2}+\\
&\sigma({B_x}^2)(\frac{\partial W_1}{\partial t}+V_{nf}VCF\frac{\partial W_1}{\partial x}))+p_i-K_wW_3+K_G\nabla^2W_3\\
&-C\frac{\partial W_3}{\partial t})=\{1-e_0a^2\nabla^2\}(\frac{N_{\theta0}}{R^2}\frac{\partial^2 W_i}{\partial\theta^2}+N_{x0}\frac{\partial^2 W_i}{\partial x^2}+I_1\frac{\partial^2 W_i}{\partial t^2})\\
&X_{11}\frac{\partial^2\Phi_i}{\partial x^2}-X_{11}\frac{l^2}{R^2}\frac{\partial^4\Phi_i}{\partial x^2\partial\theta^2}-X_{11}l^2\frac{\partial^4\Phi_i}{\partial x^4}+X_{22}\frac{\partial^2\Phi_i}{\partial\theta^2}\\
&-X_{22}\frac{l^2}{R^2}\frac{\partial^4\Phi_i}{\partial\theta^4}-X_{22}l^2\frac{\partial^4\Phi_i}{\partial x^2\partial\theta^2}-E_{31}\frac{\partial^2 W_i}{\partial x^2}-\frac{E_{31}}{R^2}\frac{\partial^2 W_i}{\partial\theta^2}\\
&+\frac{E_{31}}{R^2}\frac{\partial V_i}{\partial\theta}-X_{33}\Phi_i+E_{31}\frac{l^2}{R^2}\frac{\partial^4 W_i}{\partial x^2\partial\theta^2}+E_{31}\frac{l^2}{R^4}\frac{\partial^4 W_i}{\partial\theta^4}+\\
&E_{31}\frac{l^2}{R^2}\frac{\partial^4 W_i}{\partial x^2\partial\theta^2}-E_{31}\frac{l^2}{R^4}\frac{\partial^3 V_i}{\partial\theta^3}-E_{31}\frac{l^2}{R^2}\frac{\partial^3 V_i}{\partial x^2\partial\theta}\\
&+X_{33}\frac{l^2}{R^2}\frac{\partial^2\Phi_i}{\partial\theta^2}+X_{33}l^2\frac{\partial^2\Phi_i}{\partial x^2}=0
\end{aligned}
\tag{61}
$$

4. Solution procedure

We tackle the derived nonlocal governing differential equations via an analytical solution route. The scheme proceeds in a staged manner, invoking exact-solution apparatus to obtain explicit expressions. These forms furnish a deeper mechanistic reading of systems governed by such nonlocal models, yielding a more rounded grasp of their dynamics. Beyond strict numerical fidelity, the closed forms permit clear-eyed scans of parameters and boundary conditions, exposing how specific tunings and couplings shape system-level performance. Hence, instead of *U*, *V*, *W*, *Φ* substitute following phrases:

$$U_i=\bar{U}_ie^{j(kx+n\theta-\omega t)} \tag{62}$$

$$V_i=\bar{V}_ie^{j(kx+n\theta-\omega t)} \tag{63}$$

$$W_i=\bar{W}_ie^{j(kx+n\theta-\omega t)} \tag{64}$$

$$\Phi_i=\bar{\Phi}_ie^{j(kx+n\theta-\omega t)} \tag{65}$$

And obtained relations can be presented as:

$$[K+C\omega-M\omega^2]\begin{bmatrix}andU_i\\andV_i\\andW_i\\and\Phi_i\end{bmatrix}=0 \tag{66}$$

in which the stiffness, damping and inertia matrices of each parameter is presented as:

By setting zero the determinant of the coefficient matrix of displacement matrix, angular frequency can be obtained and the phase velocity (PV) can be computed as:

$$U_i=\bar{U}_ie^{j(kx+n\theta-\omega t)} \tag{69}$$

The proposed NSGT-based classical shell formulation offers several benefits. First, by combining nonlocal

$$
K=\begin{bmatrix}
{K_{11}}^{(1)} & {K_{12}}^{(1)} & {K_{13}}^{(1)} & {K_{14}}^{(1)}{K_{15}}^{(1)} & {K_{16}}^{(1)} & {K_{17}}^{(1)} & {K_{18}}^{(1)}{K_{19}}^{(1)} & {K_{110}}^{(1)} & {K_{111}}^{(1)} & {K_{112}}^{(1)}\\
{K_{21}}^{(1)} & {K_{22}}^{(1)} & {K_{23}}^{(1)} & {K_{24}}^{(1)}{K_{25}}^{(1)} & {K_{26}}^{(1)} & {K_{27}}^{(1)} & {K_{28}}^{(1)}{K_{29}}^{(1)} & {K_{210}}^{(1)} & {K_{211}}^{(1)} & {K_{212}}^{(1)}\\
{K_{31}}^{(1)} & {K_{32}}^{(1)} & {K_{33}}^{(1)} & {K_{34}}^{(1)}{K_{35}}^{(1)} & {K_{36}}^{(1)} & {K_{37}}^{(1)} & {K_{38}}^{(1)}{K_{39}}^{(1)} & {K_{310}}^{(1)} & {K_{311}}^{(1)} & {K_{312}}^{(1)}\\
{K_{41}}^{(1)} & {K_{42}}^{(1)} & {K_{43}}^{(1)} & {K_{44}}^{(1)}{K_{45}}^{(1)} & {K_{46}}^{(1)} & {K_{47}}^{(1)} & {K_{48}}^{(1)}{K_{49}}^{(1)} & {K_{410}}^{(1)} & {K_{411}}^{(1)} & {K_{412}}^{(1)}\\
{K_{11}}^{(2)} & {K_{12}}^{(2)} & {K_{13}}^{(2)} & {K_{14}}^{(2)}{K_{15}}^{(2)} & {K_{16}}^{(2)} & {K_{17}}^{(2)} & {K_{18}}^{(2)}{K_{19}}^{(2)} & {K_{110}}^{(2)} & {K_{111}}^{(2)} & {K_{112}}^{(2)}\\
{K_{21}}^{(2)} & {K_{22}}^{(2)} & {K_{23}}^{(2)} & {K_{24}}^{(2)}{K_{25}}^{(2)} & {K_{26}}^{(2)} & {K_{27}}^{(2)} & {K_{28}}^{(2)}{K_{29}}^{(2)} & {K_{210}}^{(2)} & {K_{211}}^{(2)} & {K_{212}}^{(2)}\\
{K_{31}}^{(2)} & {K_{32}}^{(2)} & {K_{33}}^{(2)} & {K_{34}}^{(2)}{K_{35}}^{(2)} & {K_{36}}^{(2)} & {K_{37}}^{(2)} & {K_{38}}^{(2)}{K_{39}}^{(2)} & {K_{310}}^{(2)} & {K_{311}}^{(2)} & {K_{312}}^{(2)}\\
{K_{41}}^{(2)} & {K_{42}}^{(2)} & {K_{43}}^{(2)} & {K_{44}}^{(2)}{K_{45}}^{(2)} & {K_{46}}^{(2)} & {K_{47}}^{(2)} & {K_{48}}^{(2)}{K_{49}}^{(2)} & {K_{410}}^{(2)} & {K_{411}}^{(2)} & {K_{412}}^{(2)}\\
{K_{11}}^{(3)} & {K_{12}}^{(3)} & {K_{13}}^{(3)} & {K_{14}}^{(3)}{K_{15}}^{(3)} & {K_{16}}^{(3)} & {K_{17}}^{(3)} & {K_{18}}^{(3)} & {K_{19}}^{(3)} & {K_{110}}^{(3)} & {K_{111}}^{(3)} & {K_{112}}^{(3)}\\
{K_{21}}^{(3)} & {K_{22}}^{(3)} & {K_{23}}^{(3)} & {K_{24}}^{(3)}{K_{25}}^{(3)} & {K_{26}}^{(3)} & {K_{27}}^{(3)} & {K_{28}}^{(3)} & {K_{29}}^{(3)} & {K_{210}}^{(3)} & {K_{211}}^{(3)} & {K_{212}}^{(3)}\\
{K_{31}}^{(3)} & {K_{32}}^{(3)} & {K_{33}}^{(3)} & {K_{34}}^{(3)}{K_{35}}^{(3)} & {K_{36}}^{(3)} & {K_{37}}^{(3)} & {K_{38}}^{(3)} & {K_{39}}^{(3)} & {K_{310}}^{(3)} & {K_{311}}^{(3)} & {K_{312}}^{(3)}\\
{K_{41}}^{(3)} & {K_{42}}^{(3)} & {K_{43}}^{(3)} & {K_{44}}^{(3)}{K_{45}}^{(3)} & {K_{46}}^{(3)} & {K_{47}}^{(3)} & {K_{48}}^{(3)} & {K_{49}}^{(3)} & {K_{410}}^{(3)} & {K_{411}}^{(3)} & {K_{412}}^{(3)}
\end{bmatrix}
$$

$$
M=\begin{bmatrix}
{M_{11}}^{(1)} & 0 & 0 & 0 & 0 & 0 & 0 & 0 & 0 & 0 & 0 & 0\\
0 & {M_{22}}^{(1)} & 0 & 0 & 0 & 0 & 0 & 0 & 0 & 0 & 0 & 0\\
0 & 0 & {M_{33}}^{(1)} & 0 & 0 & 0 & 0 & 0 & 0 & 0 & 0 & 0\\
0 & 0 & 0 & {M_{44}}^{(1)} & 0 & 0 & 0 & 0 & 0 & 0 & 0 & 0\\
0 & 0 & 0 & 0 & {M_{15}}^{(2)} & 0 & 0 & 0 & 0 & 0 & 0 & 0\\
0 & 0 & 0 & 0 & 0 & {M_{26}}^{(2)} & 0 & 0 & 0 & 0 & 0 & 0\\
0 & 0 & 0 & 0 & 0 & 0 & {M_{37}}^{(2)} & 0 & 0 & 0 & 0 & 0\\
0 & 0 & 0 & 0 & 0 & 0 & 0 & {M_{48}}^{(2)} & 0 & 0 & 0 & 0\\
0 & 0 & 0 & 0 & 0 & 0 & 0 & 0 & {M_{19}}^{(3)} & 0 & 0 & 0\\
0 & 0 & 0 & 0 & 0 & 0 & 0 & 0 & 0 & {M_{210}}^{(3)} & 0 & 0\\
0 & 0 & 0 & 0 & 0 & 0 & 0 & 0 & 0 & 0 & {M_{311}}^{(3)} & 0\\
0 & 0 & 0 & 0 & 0 & 0 & 0 & 0 & 0 & 0 & 0 & {M_{412}}^{(3)}
\end{bmatrix}
\tag{67}
$$

$$C = \begin{bmatrix} 0 & 0 & 0 & 0 & 0 & 0 & 0 & 0 & 0 & 0 & 0 & 0 \\ 0 & 0 & 0 & 0 & 0 & 0 & 0 & 0 & 0 & 0 & 0 & 0 \\ 0 & 0 & C_{33}{}^{(1)} & 0 & 0 & 0 & 0 & 0 & 0 & 0 & 0 & 0 \\ 0 & 0 & 0 & 0 & 0 & 0 & 0 & 0 & 0 & 0 & 0 & 0 \\ 0 & 0 & 0 & 0 & 0 & 0 & 0 & 0 & 0 & 0 & 0 & 0 \\ 0 & 0 & 0 & 0 & 0 & 0 & 0 & 0 & 0 & 0 & 0 & 0 \\ 0 & 0 & 0 & 0 & 0 & 0 & C_{37}{}^{(2)} & 0 & 0 & 0 & 0 & 0 \\ 0 & 0 & 0 & 0 & 0 & 0 & 0 & 0 & 0 & 0 & 0 & 0 \\ 0 & 0 & 0 & 0 & 0 & 0 & 0 & 0 & 0 & 0 & 0 & 0 \\ 0 & 0 & 0 & 0 & 0 & 0 & 0 & 0 & 0 & 0 & 0 & 0 \\ 0 & 0 & 0 & 0 & 0 & 0 & 0 & 0 & 0 & C_{311}{}^{(3)} & 0 & 0 \\ 0 & 0 & 0 & 0 & 0 & 0 & 0 & 0 & 0 & 0 & 0 & 0 \end{bmatrix} \tag{68}$$

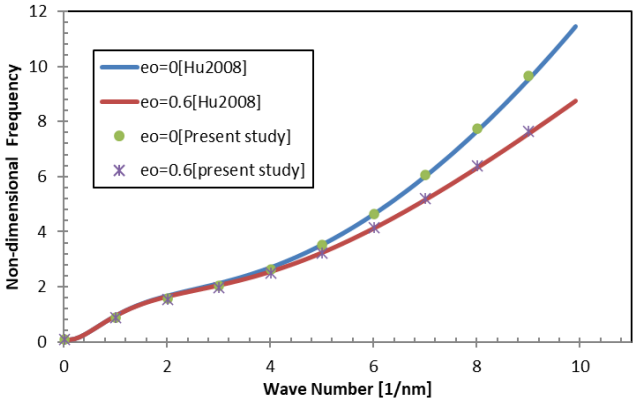

Fig. 3 Illustration of non-dimensional frequency against wave number compare with reference (Hu *et al*. 2008)

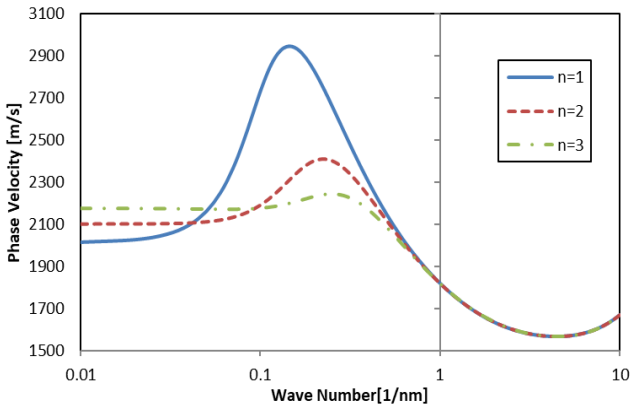

Fig. 4 Illustration of PV of TWBNNT against wave number for various modes

parameter (e_0a) and length-scale parameter (l) measures, it remains accurate from long to short wavelengths, avoiding the stiffness bias of purely local theories. Second, electro-magneto-thermal loading and rarefied internal flow (via VCF) are coupled at the operator level, yielding a single closed-form dispersion relation in which field interactions appear transparently. Third, inter-wall Van der Waals forces are retained for TWBNNTs, capturing interlayer coupling effects that materially influence phase-velocity trends. Fourth, the inclusion of a viscoelastic Winkler–Pasternak foundation with damping provides a realistic substrate model for embedded nano-conduits. Finally, the analytical structure of the dispersion equation enables efficient parametric studies and clear limit checks (local/nonlocal), while our results reproduce a benchmark nonlocal shell trend over the full k R range reported (Fig. 3), supporting both fidelity and computational economy.

5. Results and discussion

Firstly, it is tried to validate the accuracy of the employing methodology. Hence, the obtained outcomes are verified with the results of investigation presented by Hu *et al*. (2008). Their results verified by molecular dynamics. The comparison depicts the good agreement between the results of this investigation with those reported by Hu *et al*. (2008). Fig. 3 indicates non-dimensional frequency against wave number. Non-dimensional frequency for drawing this diagram is regarded as $\Omega = \omega L\sqrt{\frac{I_1}{A_{11}}}$. The considered geometry of BNNT is (Salehi-Khojin and Jalili, 2008):

$$\begin{aligned} &R_1 = 11.43nm, \quad R_2 = 12.31nm, \\ &R_3 = 13.2nm, \quad \frac{L}{R_1} = 10, h = 0.075nm, \\ &\rho = 3.4870g/cm^3 \end{aligned} \tag{70}$$

As shown in Fig. 3, the local and nonlocal formulations essentially coalesce in the low-wavenumber regime. Beyond this cutoff, however, the nondimensional frequency predicted by the local model (under the stated parameter setting) undershoots the nonlocal prediction. Moreover, the nonlocal results are in close, near one-to-one accord with the molecular-dynamics benchmarks.

Variation of PV of TWBNNT as a function of wave number for dissimilar modes is shown in Fig. 4. As expected, PV reaches to its maximum amount in first mode. By rising wave number, PV enlarges to its peak and then is reduced. Once wave number equals 0.01 (1/nm) PV of higher mode is bigger than another. After wave number 1(1/nm) charts leads to an identical amount.

Table 2 illustrates changes of velocity and frequency of propagated waves in TWBNNT against wave number for dissimilar fluid velocities. As observed, in constant fluid velocity for different wave numbers, frequency enlarges and PV in each case has different trend that to come to correct

Table 2 PV and wave frequency of TWBNNT for dissimilar fluid velocities and wave numbers

Fluid velocity [m/s]	Wave number [1/nm]	PV [m/s]	Wave frequency [THz]
100	0. 1	360.307	0.0360307
100	1	848.65	0.84865
100	10	839.974	8.39974
500	0. 1	1578.61	0.157861
500	1	1265.44	1.26544
500	10	1214.71	12.1471
1000	0. 1	2731.4	0.27314
1000	1	1819.07	1.81907
1000	10	1668.96	16.6896

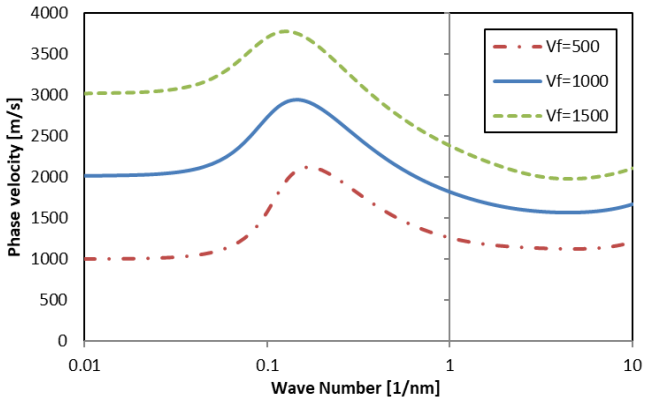

Fig. 5 Illustration of the effect of fluid velocity on PV of TWBNNT against wave number

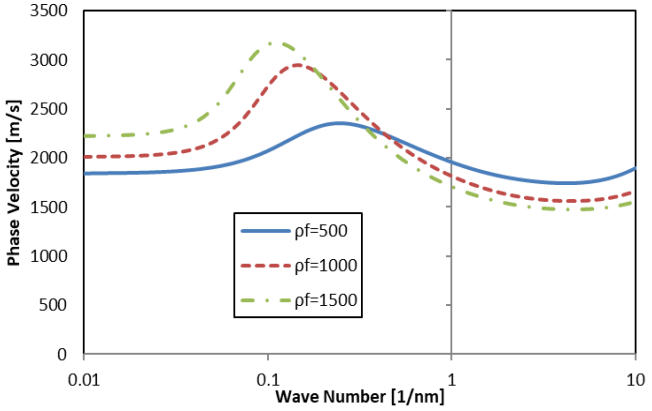

Fig. 6 Illustration of the effect of fluid density on PV of TWBNNT against wave number

conclusion, it should be exist more points for sampling. Moreover, for constant wave number with increasing fluid velocity, PV and frequency increases.

The effects of fluid density on changes of PV of TWBNNT versus wave number is presented in Fig. 6. As is observable, trend at first is ascending then is descending. By rising fluid density, the peak of diagram becomes greater and this peak occurs in smaller wave number. For smaller wave number 108 (1/m) by rising fluid density, PV increases but after this wave number trend becomes reverse.

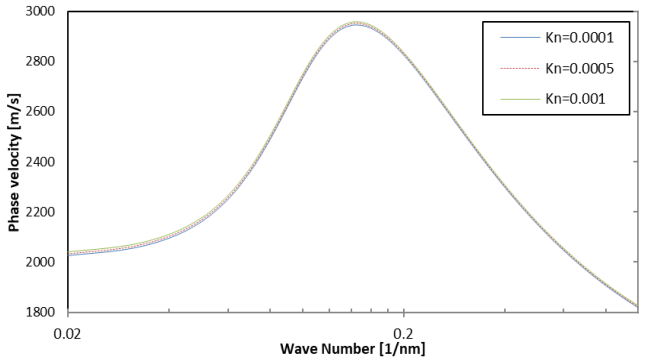

Fig. 7 Illustration of PV of TWBNNT as a function of wave number for various Knudsen numbers

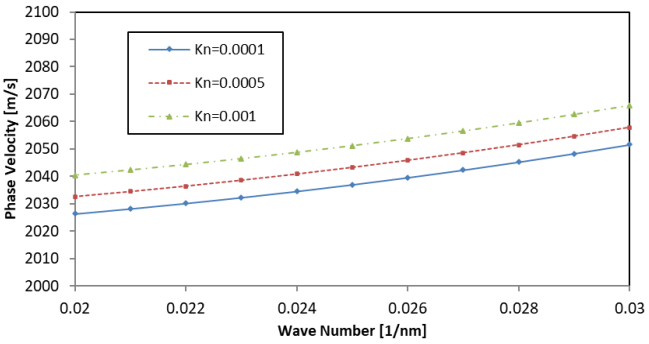

Fig. 8 The magnified illustration of PV of TWBNNT against wave number for various Knudsen numbers

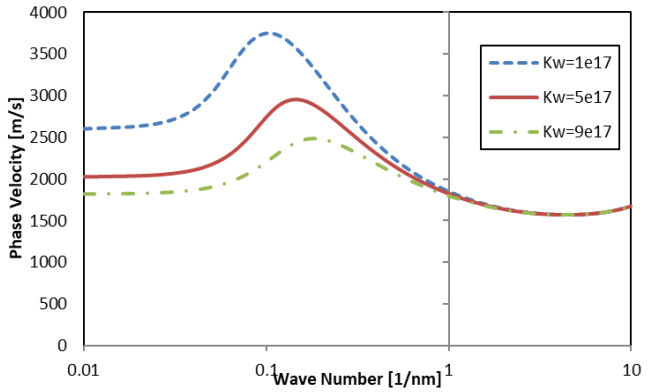

Fig. 9 Illustration of influence of Winkler coefficient on PV of TWBNNT against wave number

Fig. 7 demonstrates how Knudsen numbers affect PV for different wave number. In this diagram, there is very little deviation of PV for different Knudsen numbers and approximately have an identical PV. A little difference can be seen in smaller wave numbers that is indicated in magnified diagram of Fig. 8. According to Fig. 8, by rising Knudsen number, PV increases that is almost 10 (m/s).

The effect of viscoelastic foundation includes three Winkler, damping and Pasternak coefficient that the effect of each coefficient will be analyzed distinctly. The effect of Winkler coefficient on variation of PV versus wave number of TWBNNT is reported in Fig. 9. For smaller wave number than 10^9 (1/m) by rising Winkler coefficient, PV is reduced. Slope of this diagram is ascending at first then

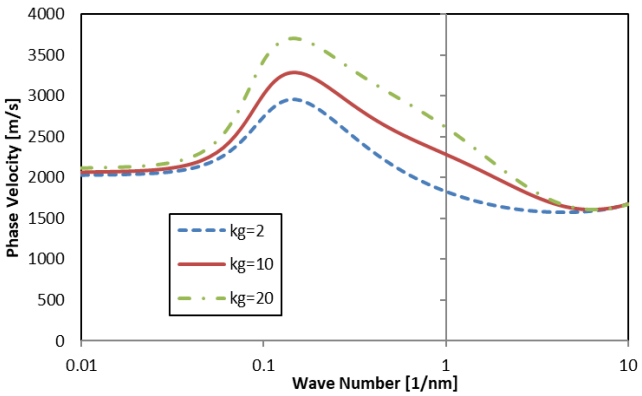

Fig. 10 Illustration of PV of TWBNNT against wave number for dissimilar Pasternak coefficients

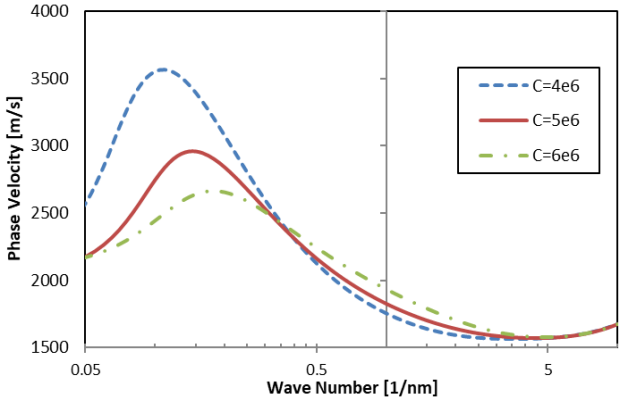

Fig. 11 Illustration of PV of TWBNNT as a function of wave number for various damping coefficients

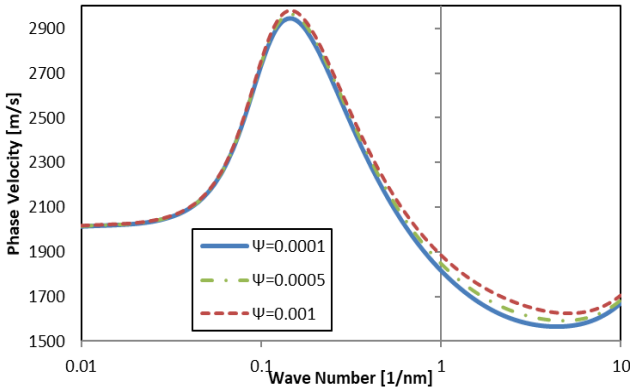

Fig. 12 Illustration of effect of magnetic field intensity on PV of TWBNNT for different wave numbers

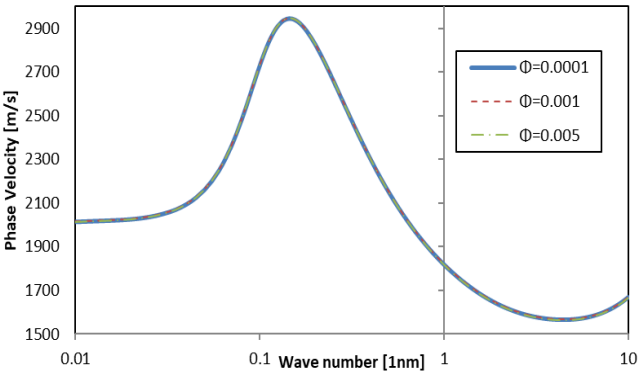

Fig. 13 Illustration of the effect of electric field intensity on PV of TWBNNT for different wave numbers

Table 3 PV of TWBNNT for dissimilar wave number and electric field intensity

Electric field intensity (V)	Wave number [1/nm]	PV [m/s]	Wave frequency [THz]
0.0001	0.01	2014.38	0.0201438
	0.1	2731.4	0.27314
	0.5	2152.7	1.07635
	1	1819.07	1.81907
	10	1668.66	16.6866
0.001	0.01	2014.37	0.0201437
	0.1	2731.35	0.273135
	0.5	2152.61	1.076305
	1	1818.95	1.81895
	10	1668.58	16.6858
0.005	0.01	2014.34	0.0201434
	0.1	2731.12	0.273112
	0.5	2152.18	1.07609
	10	1668.26	16.6826

becomes descending. In addition, by rising Winkler coefficient amount of peak and ascending slope and descending slope is decreased and this increasing causes damping state is created. For bigger Winkler coefficient, diagram tends to a direct line. Also, for bigger wave numbers, changing Winkler coefficient make no change in PV.

The influence of Pasternak coefficient on PV of TWBNNT against wave number is shown in Fig. 10. Diagram at first has uptrend and afterwards with downtrend reaches to constant amount smaller than initial amount. As observed, by rising Pasternak coefficient, PV enlarges. All diagrams at last leads to a constant amount.

Fig. 11 indicates the sensitivity of PV of TWBNNT on

Table 4 Variation of PV of TWBNNT as a function of wave number and temperature difference

Temperature difference (℃)	Wave number [1/nm]	PV [m/s]	Wave frequency [THz]
10	0.01	2014.38	0.0201438
	0.1	2731.4	0.027314
	0.5	2152.7	1.07635
	1	1819.07	1.81907
	10	1668.66	16.6866
50	0.01	2014.37	0.0201437
	0.1	2731.32	0.0273132
	0.5	2152.55	1.076275
	1	1818.86	1.81886
	10	1668.54	16.6854
100	0.01	2014.35	0.0201435
	0.1	2731.21	0.0273121
	0.5	2152.35	1.076175
	1	1818.6	1.8186

damping coefficients. The wave number changes are considered in range of 0.05 [1/nm] to 10 [1/nm]. If this range divided to three parts, in first range 0.05 to 0.5 [1/nm] with increasing damping coefficient, PV is decreased and the peak of diagram is in this range. In second range 0.5 to 5 [1/nm] by rising damping coefficient, PV increases and difference into diagrams becomes less. In the last range PV of each damping coefficient becomes identical amount.

Influences of electric and magnetic fields on PV of TWBNNT are illustrated in Fig. 12-13. As can be seen in Fig. 12, in smaller wave numbers diagrams are identical but in higher wave numbers by rising magnetic field intensity PV increases. It is clear that difference between diagrams for various electric field intensities is very slight. Thus, for showing this difference, several number of it is brought in Table 3.

Table 3 presented the effect of electric field intensity on variation of wave frequency and PV of TWBNNT for various wave numbers. As is observable while electric filed intensity increases, PV and wave frequency are lessened. As well as previous diagrams, wave number has positive and negative effect and depends on its value.

Effect of thermal field on PV of TWBNNT versus wave number is demonstrated in Table 4. As observed, for constant temperature difference, PV enlarges at first but at continue has downtrend. Also, by rising temperature difference, PV is decreased. This is due to softening effect of thermal field. Indeed, in greater temperature, the stiffness of structure is lessened and leads to lower wave frequency and PV.

6. Conclusions

Wave propagation of fluid-conveying TWBNNT lying on viscoelastic medium under multi-physical fields was investigated based on NSGT employing CS theory. The main findings of the current study are:

• Model validation: The nonlocal formulation reproduces the benchmark trend across the full wavenumber range, the local theory underestimates frequency at higher k. (Fig. 3).

• Mode effect: Phase velocity (PV) peaks in the first mode, with increasing k, PV rises to a maximum and then declines, beyond $k \approx 1$ nm^{-1} the modes converge. (Fig. 4).

• Fluid velocity: At fixed k, increasing internal flow speed increases both PV and wave frequency. (Table 2, Fig. 5).

• Fluid density: PV increases with fluid density at small wavenumbers (around 10^8 m^{-1}) but decreases at larger k, the PV peak shifts toward smaller k as density grows. (Fig. 6).

• Knudsen (rarefaction): Knudsen effects are modest overall, at small k a higher Kn slightly raises PV (≈10 m/s). (Figs. 7–8).

• Foundation parameters:

a) Winkler stiffness lowers PV at small k, effect vanishes at large k. (Fig. 9).

b) Pasternak shear raises PV, with curves tending to a common limit at large k. (Fig. 10).

c) Damping shows three regimes: PV decreases with damping for $0.05 \leq k \leq 0.5$ nm^{-1}, increases for $0.5 \leq k \leq 5$ nm^{-1}, and coalesces for $5 \leq k \leq 10$ nm^{-1}. (Fig. 11).

• External fields: Stronger magnetic field increases PV at higher k, electric field slightly reduces PV, thermal increase (ΔT) softens the system and reduces PV. (Figs. 12–13, Tables 3–4).

Collectively, these trends quantify how internal flow, rarefaction, substrate mechanics, and electro-magneto-thermal fields can be used to tune guided-wave transport in fluid-conveying TWBNNTs on viscoelastic media.

References

Abdellahi, R., Jabbari, M. and Shamshiri, A. (2024), "Investigation of free vibration of piezoelectric actuator reinforced with

functionally graded Boron Nitride nanotube using timoshenko beam model and differential quadrature method", *Results Eng*., **23**, 102374. https://doi.org/10.1016/j.rineng.2024.102374.

Abdollahian, M., Arani, A.G., Barzoki, A.M., Kolahchi, R. and Loghman, A. (2013), "Non-local wave propagation in embedded armchair TWBNNTs conveying viscous fluid using DQM", *Physica B Condensed Matter*, **418**, 1-15. https://doi.org/10.1016/j.physb.2013.02.037.

Ansari, R., Rouhi, S. and Nikkar, A. (2017), "Finite element investigation of the vibrational behavior of concentric multi-walled boron nitride and carbon nanotubes", *Int. J. Modern Phys. B*, **31**(4), 1750018. https://doi.org/10.1142/S0217979217500187.

Arani, A.G. and Roudbari, M. (2014), "Surface stress, initial stress and Knudsen-dependent flow velocity effects on the electro-thermo nonlocal wave propagation of SWBNNTs", *Physica B Condensed Matter*, **452**, 159-165. https://doi.org/10.1016/j.physb.2014.07.017.

Arani, A.G., Shajari, A., Amir, S. and Loghman, A. (2012), "Electro-thermo-mechanical nonlinear nonlocal vibration and instability of embedded micro-tube reinforced by BNNT, conveying fluid", *Physica E*, **45**, 109-121. https://doi.org/10.1016/j.physe.2012.07.017.

Aydin, M. (2013), "Vibrational and electronic properties of single-walled and double-walled boron nitride nanotubes", *Vib. Spectrosc*., **66**, 30-42. https://doi.org/10.1016/j.vibspec.2013.01.011.

Badehian, H.A. and Vatankhah, C. (2022), "Structural and optical behavior of single-walled and multi-walled boron nitride nanotubes", *J. Mol. Struct*., **1262**, 133069. https://doi.org/10.1016/j.molstruc.2022.133069.

Chandra, A., Patra, P. K. and Bhattacharya, B. (2015), "Thermal vibration characteristics of armchair boron-nitride nanotubes", *J. Appl. Phys*., **118**(23). https://doi.org/10.1063/1.4937559.

Choyal, V. and Kundalwal, S. (2020), "Transversely isotropic elastic properties of multi-walled boron nitride nanotubes under a thermal environment", *Nanotechnology*, **31**(39), 395707. https://doi.org/10.1088/1361-6528/ab9865.

Dong, K., Zhu, S. and Wang, X. (2008), "Wave propagation in multiwall carbon nanotubes embedded in a matrix material", *Compos. Struct*., **82**(1), 1-9. https://doi.org/10.1016/j.compstruct.2006.11.003.

Ebrahimi, F. and Seyfi, A. (2022), "Wave propagation analysis of smart inhomogeneous piezoelectric nanosize beams rested on an elastic medium", *Waves Random Complex Med*., **32**(3), 1269-1288. https://doi.org/10.1080/17455030.2020.1817625.

Ebrahimi, F. and Seyfi, A. (2023), "Wave dispersion analysis of embedded MWCNTs-reinforced nanocomposite beams by considering waviness and agglomeration factors", *Waves Random Complex Med*., **33**(3), 525-544. https://doi.org/10.1080/17455030.2021.1883148.

Ebrahimi, F., Seyfi, A. and Dabbagh, A. (2019a), "Dispersion of waves in FG porous nanoscale plates based on NSGT in thermal environment", *Adv. Nano Res*., **7**(5), 325-335. https://doi.org/10.12989/anr.2019.7.5.325.

Ebrahimi, F., Seyfi, A. and Dabbagh, A. (2019b), "A novel porosity-dependent homogenization procedure for wave dispersion in nonlocal strain gradient inhomogeneous nanobeams", *Eur. Phys. J. Plus*, **134**(5), 226. https://doi.org/10.1140/epjp/i2019-12547-8.

Ebrahimi, F., Dehghan, M. and Seyfi, A. (2019c), "Eringen's nonlocal elasticity theory for wave propagation analysis of magneto-electro-elastic nanotubes", *Adv. Nano Res*., **7**(1), 1. https://doi.org/10.12989/anr.2019.7.1.001.

Ebrahimi, F., Seyfi, A. and Teimouri, A. (2023), "Torsional vibration analysis of scale-dependent non-circular graphene oxide powder-strengthened nanocomposite nanorods", *Eng. Comput*., 1-12. https://doi.org/10.1007/s00366-021-01528-y.

Esen, I., Aktaş, K.G. and Pehlivan, F. (2025), "Investigation of the critical buckling temperatures and free vibration response of porous functionally graded magneto-electro-elastic sandwich higher-order nanoplates with temperature-dependent material properties", *J. Vib. Eng. Tech*., **13**(2), 1-29. https://doi.org/10.1007/s42417-024-01542-6.

Ghorbanpour-Arani, A., Rastgoo, A., Hafizi Bidgoli, A., Kolahchi, R. and Ghorbanpour Arani, A. (2017), "Wave propagation of coupled double-DWBNNTs conveying fluid-systems using different nonlocal surface piezoelasticity theories", *Mech. Adv. Mater. Struct*., **24**(14), 1159-1179. https://doi.org/10.1080/15376494.2016.1227488.

Gopalakrishnan, S. and Narendar, S. (2013), *Wave Propagation in Nanostructures*, Nonlocal Continuum Mechanics Formulations. https://doi.org/10.1007/978-3-319-01032-8.

Hu, Y.G., Liew, K. M., Wang, Q., He, X. and Yakobson, B. (2008), "Nonlocal shell model for elastic wave propagation in single- and double-walled carbon nanotubes", *J. Mech. Phys. Solids*, **56**(12), 3475-3485. https://doi.org/10.1016/j.jmps.2008.08.010.

Jakubinek, M., Martinez-Rubi, Y., Ashrafi, B., Guan, J., Kim, K., O'Neill, K., ... Simard, B. (2015), "Polymer nanocomposites incorporating boron nitride nanotubes", *Proceedings of the Nanotech 2015 Conference*, Washington, DC, USA.

Mitra, M. and Gopalakrishnan, S. (2009), "Wave propagation in multi-walled carbon nanotube", *Comput. Mater. Sci*., **45**(2), 411-418. https://doi.org/10.1016/j.commatsci.2008.10.022.

Mohammadimehr, M., Farsi, A.A., Eslami Farsani, R., Dashti Gohari, P. and Yousefi Ramandi, M. (2015), "The surface stress effects on linear vibration of nonlocal triple-walled boron nitride nano tube conveying viscose fluid flow using DQM", *J. Model. Eng*., **13**(43), 47-66. https://sid.ir/paper/173846/en.

Nikkar, A., Rouhi, S. and Ansari, R. (2019), "On the buckling properties of concentric carbon/boron-nitride multi-walled nanotubes: a finite element investigation", *Mech. Adv. Mater. Struct*., **26**(9), 816-824. https://doi.org/10.1080/15376494.2018.1430259.

Oveissi, S. and Nahvi, H. (2015), "Transverse vibration and instability of fluid conveying triple-walled carbon nanotubes based on strain-inertia gradient theory", *J. Theor. Appl. Vib. Acoust*., **1**(2), 62-72. https://doi.org/10.22064/tava.2015.13645.

Roodgar Saffari, P., Fakhraie, M. and Roudbari, M.A. (2022), "Free vibration problem of fluid-conveying double-walled boron nitride nanotubes via nonlocal strain gradient theory in thermal environment", *Mech. Based Des. Struct*., **50**(10), 3665-3682. https://doi.org/10.1080/15397734.2020.1819310.

Salehi-Khojin, A. and Jalili, N. (2008), "Buckling of boron nitride nanotube reinforced piezoelectric polymeric composites subject to combined electro-thermo-mechanical loadings", *Compos. Sci. Tech*., **68**(6), 1489-1501. https://doi.org/10.1016/j.compscitech.2007.10.024.

Sedighi, H.M., Ouakad, H.M., Dimitri, R. and Tornabene, F. (2020), "Stress-driven nonlocal elasticity for the instability analysis of fluid-conveying C-BN hybrid-nanotube in a magneto-thermal environment", *Physica Scripta*, **95**(6), 065204. https://doi.org/10.1088/1402-4896/ab793f.

Seyfi, A. and Aghdam, M. (2023), "Vibrational behavior of temperature-dependent imperfect functionally graded plate lying on an elastic substrate", *Mech. Based Des. Struct*., **51**(7), 3868-3889. https://doi.org/10.1080/15397734.2021.1944189.

Seyfi, A., Teimouri, A., Dimitri, R. and Tornabene, F. (2022), "Dispersion of elastic waves in functionally graded CNTs-reinforced composite beams", *Appl. Sci*., **12**(8), 3852. https://doi.org/10.3390/app12083852.

Seyfi, A., Teimouri, A. and Ebrahimi, F. (2024), "Scale-dependent torsional vibration response of non-circular nanoscale auxetic rods", *Waves Random Complex Med*., **34**(5), 4425-4441.

https://doi.org/10.1080/17455030.2021.1990441.
Sobhy, M. (2025), "Nonlinear bending and vibration of FGCNTs cylindrical microshells conveying microfluid under a 2D magnetic field", *Arch. Civil Mech. Eng.*, **25**(4), 1-38. https://doi.org/10.1007/s43452-025-01212-8.
Taati, E. and Ahmadian, M. (2023), "Thermoelastic resonance analysis of BNNT-reinforced nanocomposite beams heated by internal thermal source", *Structures*, **55**, 1011-1027.
Taghizadeh, M., Askari, A.R. and Farzinpoor, H. (2025), "Size-dependent finite element buckling analysis of porous cylindrical micro-shells reinforced by graphene platelets", *Mech. Based Des. Struct.*, **53**(3), 2152-2181. https://doi.org/10.1080/15397734.2024.2404606.
Thibeault, S.A., Kang, J.H., Sauti, G., Park, C., Fay, C.C. and King, G.C. (2015), "Nanomaterials for radiation shielding", *Mrs Bulletin*, **40**(10), 836-841. https://doi.org/10.1557/mrs.2015.225.
Yan, J., Tong, L. and Xiang, P. (2017), "Free vibration analysis of single-walled boron nitride nanotubes based on a computational mechanics framework", *Superlatt. Microstruct.*, **112**, 230-248. https://doi.org/10.1016/j.spmi.2017.09.028.
Zeighampour, H., Beni, Y.T. and Dehkordi, M.B. (2018), "Wave propagation in viscoelastic thin cylindrical nanoshell resting on a visco-Pasternak foundation based on nonlocal strain gradient theory", *Thin Wall. Struct.*, **122**, 378-386. https://doi.org/10.1016/j.tws.2017.10.037.

CC